# Frequency-Domain Method for the Computation of Propeller Acoustics

J. B. H. M. Schulten*
*National Aerospace Laboratory NLR, Amsterdam, the Netherlands*

**In the present study an analytical description of the acoustic field of a propeller in a uniform flow is derived. Instead of applying the usual Ffowcs-Williams-Hawkings version of the acoustic analogy, here we formulate sources on a surface enclosing the propeller and its adjacent nonlinear flowfield. This approach, which avoids the laborious evaluation of quadrupole source terms, is to be considered as a generalization of the Kirchhoff-Helmholtz theorem of acoustics. By describing the fundamental solution as a spectral Fourier-Bessel decomposition, the resulting sound field is readily given in the appropriate series of harmonic amplitudes. The method is validated by a comparison of numerical results with experimental data of a propeller in an acoustic wind tunnel. A good agreement both in amplitude and phase is found between theory and experiment.**

## Nomenclature

$a_n(\alpha, \gamma, r)$ = $[\alpha, -i\gamma J_n'(\gamma r)/J_n(\gamma r), n/r]$
$a_n^*(\alpha, \gamma, \rho)$ = $[\alpha, i\gamma J_n'(\gamma\rho)/J_n(\gamma\rho), n/\rho]$
$B$ = number of blades
$b_n(x-\xi, r, \gamma, \omega)$ = $a_n\{[M\omega - \mathrm{sgn}(x-\xi)\kappa(\gamma, \omega)]/\beta^2, \gamma, r\}$
$b_n^*(x-\xi, \rho, \gamma, \omega)$ = $a_n^*\{[M\omega - \mathrm{sgn}(x-\xi)\kappa(\gamma, \omega)]/\beta^2, \gamma, \rho\}$
$c_n(r, \gamma, \omega)$ = $a_n(-\omega/M, \gamma, r)$
$c_n^*(\rho, \gamma, \omega)$ = $a_n^*(-\omega/M, \gamma, \rho)$
$F$ = force field
$f$ = surface force distribution
$G$ = Green's function
$g(x, r)$ = $\left(-r\frac{\partial\varphi_0}{\partial x}, -r\frac{\partial\varphi_0}{\partial r}, 1\right)$ normal to blade surface
$i_x, i_r, i_\theta$ = unit vectors in $x$, $r$, $\theta$ directions, respectively (Fig. 3)
$J_n, J_n'$ = Bessel function of the first kind and order $n$, its derivative
$j$ = blade index
$k$ = circumferential Fourier index of distortion velocity component
$\ell$ = index of discrete frequency at $S = 0$
$M$ = main flow Mach number
$m$ = $k - nB$
$n, N$ = harmonic index
$p$ = pressure
$Q$ = displacement source strength
$q$ = surface distribution of $Q$
$r$ = radial coordinate
$S$ = function to define a surface (Eq. 1)
$t$ = time coordinate
$v$ = velocity induced by propeller
$w$ = incident distortion velocity
$x$ = axial coordinate (Fig. 3)
$\alpha$ = axial wave number
$\beta$ = $\sqrt{1-M^2}$
$\beta_{0.7}$ = blade reference angle
$\gamma$ = radial wave number
$\theta$ = angular coordinate (Fig. 3)
$\kappa(\gamma, \omega)$ = $\sqrt{\omega^2 - \beta^2\gamma^2}$ (see Eq. 13)
$\xi$ = axial source coordinate
$\rho$ = radial source coordinate
$\tau$ = source time coordinate, local variable
$\varphi$ = angular source coordinate, local variable
$\varphi_0$ = angular blade surface coordinate of zeroth blade at $t = 0$
$\Omega$ = circumferential tip Mach number
$\omega$ = Helmholtz number (nondimensional radian frequency)
$\omega_{\ell,k}$ = $\omega_\ell - k\Omega$
$\omega_\ell$ = $\ell$th discrete frequency at $S = 0$
$\omega_n$ = $\omega_{\ell,k} + nB\Omega$
$< \cdot >$ = inner product of two three-dimensional vectors
$\nabla_0$ = gradient operator in source coordinates

*Subscripts*

$F$ = force
$Q$ = displacement

*Superscripts*

$\sim$ = in time domain
$\hat{}$ = axially Fourier-transformed variable
$\bar{}$ = radially Hankel-transformed variable
$(\,)^\ell$ = (blade) lower surface (Fig. 4)
$(\,)^u$ = (blade) upper surface (Fig. 4)

Received Aug. 21, 1987; presented as Paper 87-2674 at the AIAA 11th Aeroacoustics Conference, Sunnyvale, CA, Oct. 19-21, 1987; revision received Feb. 8, 1988. 

*Senior Research Engineer, Department of Fluid Dynamics. Member AIAA.

## Introduction

In the past decade, aerodynamic research has shown the feasibility of advanced propellers for the high-subsonic flight regime with a superior fuel economy compared to turbofan propulsion. Unfortunately, these high-speed propeller systems tend to be considerably more noisy because of the absence of a duct to shield and attenuate the sound generated by the blades. Therefore, the aeroacoustical challenge in the application of these propellers is to minimize their noise impact without spoiling their favorable propulsion efficiency. Significant progress has been made so far. Careful tailoring of blade sweep has already been shown quite effective in reducing the peak noise level.[1] Of course, the position of the propeller system relative to the aircraft is also an important parameter with which to control the noise, in particular the cabin noise level.

Any optimization procedure of the acoustics of a propeller system will almost inevitably require the calculation of the acoustic pressure in a large number of field points. The present paper describes a method to calculate these pressures

efficiently. This method may be considered an alternative to other theories. The differences of the present method with Farassat's[2] and Hanson's[3] theory will be discussed next and in the section that follows. The method is validated by comparison with detailed experiments carried out in the German–Dutch wind tunnel DNW.

In modern propeller acoustic theory it has become a tradition to take Ffowcs-Williams and Hawkings' (FW-H) extension[4] of Lighthill's[5] acoustic analogy concept as the starting point. In this general formulation, the acoustic field of a body, moving in a locally nonuniform, unsteady flowfield, is expressed in terms of a monopole and a dipole source distribution over the body surface and a quadrupole source distribution over the volume containing the nonuniform, unsteady field in which the body travels (Fig. 1). Here, the quadrupole source terms correspond to the nonlinearities in the flow equations. At a large distance, the medium is at rest, apart from perturbations of acoustic order. Thus, to be able to evaluate the quadrupole source terms, it is in principle necessary to know the complete flowfield around the body in advance. Although formally exact, a direct evaluation requires an extremely high numerical accuracy of the computed flowfield because of the occurrence of double derivatives of the flow variables in the quadrupole terms.

Therefore, it is worthwhile to seek an alternative formulation in which the acoustic field generated by a certain volume that contains acoustic source strength is written in terms of the flow variables at the surface that bounds the volume. This must be possible since any change within the volume is not felt in the outer field as long as the conditions at the surface remain unchanged. Indeed, for a medium at rest at infinity, the classical Kirchhoff–Helmholtz (K-H) theorem (e.g., Ref. 6) is such a formulation. Ffowcs-Williams and Hawkings[4] indicate this theorem briefly as an alternative to their acoustic analogy concept. They consider it less applicable for the case of turbulence interacting with surfaces. However, in actual deterministic calculations, as for propellers, the K-H approach is more efficient for two reasons. First, a surface integral has to be evaluated instead of a volume integral, and second, the cumbersome calculation of the rather complicated quadrupole terms is avoided. Only pressure and velocity, and not derivatives of them, occur in the K-H formulation.

In the present study, we will therefore follow the second approach and derive a generalized version of the K-H theorem in a uniform flow rather than in a medium at rest since this is more appropriate for propellers in uniform forward motion. It will be shown that, in general, not only an acoustic field is generated at the boundary but also a hydrodynamic, vortical velocity field.

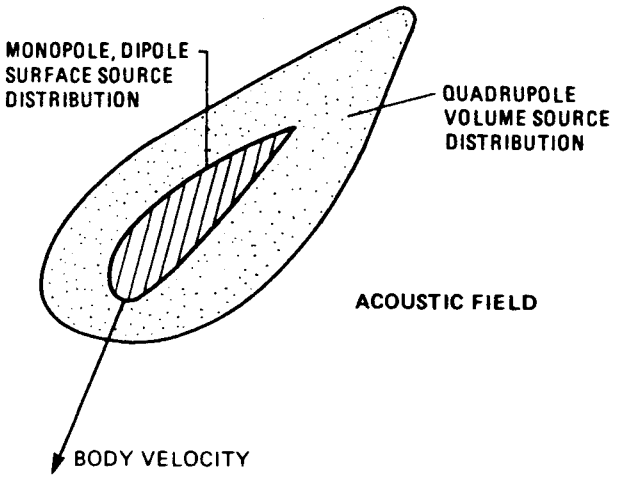


**Fig. 1 Acoustic analogy for a moving body in fluid at rest.**

It may be noted that the K-H formulation does not imply any loss of insight into the distribution of acoustic source strength. For example, to find the acoustic source strength of a certain small part of the total source volume, a K-H integral is to be taken over the surface of that part. Or to find the contribution of the quadrupole sources to the total acoustic field, one simply takes the difference of the K-H integral over a surface enclosing all acoustic source strength and the K-H integral over the body surface.

Recently, the merits of the K-H formulation have also been recognized and used by Lyrintzis and George[7] and Isom et al.[8] in the modeling of rotor aeroacoustics. Likewise, the advantage of converting the volume quadrupole integrals into surface integrals is mentioned by Farassat.[9]

In many operating conditions of propellers, in particular when the efficiency is high, i.e., the induced velocity perturbations are small, the quadrupole field is relatively weak and can be neglected. Then the two methods coincide since in the FW-H modeling the field sources vanish, whereas in the present method the source surface "shrinks" to the actual blade surfaces. In the numerical examples here, the latter simplification has been adopted. For conditions with a nonnegligible quadrupole source field, it is straightforward to apply the present method with source surfaces ($S = 0$) at some distance from the blade surface, provided the aerodynamic field is given. On the other hand, inclusion of the quadrupole strength in the FW-H formulation for propellers implies considerable additional analytical and numerical effort.

Irrespective of the approach followed, we need a Green's function, or fundamental solution, of the problem considered. Roughly speaking, there are two ways to express the Green's function for the present problem, each having its own merits and drawbacks. Both describe the acoustic field of an impulsive point source but have an entirely different appearance. The first one perhaps is the most appealing physically since it clearly displays the spherical propagation of an acoustic pulse modified by mean flow convection. This representation leads to the so-called time-domain method, first applied in propeller acoustics by Gutin[10] in 1936 and since then frequently used in this context. Farassat's method[2] is a modern version of the time-domain approach. The second representation of the Green's function naturally emerges by taking Fourier-Hankel transforms of the governing equation. Then we obtain an alternative representation in separated, cylindrical coordinates that leads to a so-called frequency (and wave number) domain method (e.g., Hanson,[3] present method). An advantage of this approach is that the final solution of the propeller acoustic field automatically yields an expansion in time-space harmonics that is most appropriate in acoustic applications. Also, the description of propeller blades is easier in cylindrical than in spherical coordinates. And finally, integrations have to be performed for one single blade only since the combined effect of all blades can be taken into account analytically.

Since the sound field of a propeller is significantly affected by asymmetries in the inflow,[11,12] the present theory includes the possibility of a nonuniform incident field. Examples of such an incident field are the upwash in which propellers operate in front of a wing, airframe wakes impinging on pusher propellers, and the mutual aerodynamic interference between the front and aft rotor of a dual counter-rotation propeller system.

The comparison with experiments in the present paper, however, has been limited to uniform, axisymmetric inflow conditions. To obtain the required blade surface pressures, a well-established two-dimensional method[13] for the propeller section aerodynamics coupled with blade element momentum theory[14] was used. For the conventional, unswept propeller used in the experiment, this procedure is expected to yield a reasonable approximation for the global aerodynamics. However, in the propeller tip region, where three-dimensional effects are important, the accuracy may be less.

## Analysis

### Governing Equations

Let $S(\boldsymbol{x}, t) = 0$ describe a surface enclosing a body moving in a uniform flow such that outside $S = 0$ the field is, to leading order, governed by the linearized flow equations for the perturbations $(\tilde{p}, \tilde{v})$ induced by the body. Further, let $S < 0$ inside $S = 0$ and $S > 0$ outside (Fig. 2). Then choosing the $x$ axis parallel to the main flow direction, we can make the linearized flow equations formally valid throughout space by multiplying them with $H(S)$, the Heaviside function of $S$, as follows:

$$H(S)\left[\frac{\mathrm{D}}{\mathrm{D}t}\tilde{p} + \nabla\cdot\tilde{v}\right] = 0 \tag{1}$$

$$H(S)\left[\frac{\mathrm{D}}{\mathrm{D}t}\tilde{v} + \nabla\tilde{p}\right] = 0 \tag{2}$$

where $\mathrm{D}/\mathrm{D}t = (\partial/\partial t) + M(\partial/\partial x)$. These equations have been made dimensionless by taking a typical length of the body, the mass density, and speed of sound of the fluid at infinity as scaling parameters. Rearrangement of Eqs. (1) and (2) yields the following equations for pressure and velocity outside $S = 0$

$$\frac{\mathrm{D}}{\mathrm{D}t}[\tilde{p}H(S)] + \nabla\cdot[\tilde{v}H(S)] = \tilde{Q}\,\delta(S) \tag{3}$$

$$\frac{\mathrm{D}}{\mathrm{D}t}[\tilde{v}H(S)] + \nabla\,[\tilde{p}H(S)] = \tilde{F}\,\delta(S) \tag{4}$$

where

$$\tilde{Q} = \tilde{p}\,\frac{\mathrm{D}S}{\mathrm{D}t} + <\tilde{v}\cdot\nabla S>$$

$$\tilde{F} = \tilde{v}\,\frac{\mathrm{D}S}{\mathrm{D}t} + \tilde{p}\nabla S$$

Physically, $\tilde{Q}$ can be interpreted as the displacement and $\tilde{F}$ as the force applied by the surface $S = 0$ to the surrounding fluid. Note that $\tilde{F}$ and $\tilde{Q}$ are defined differently from Ref. 18.

Elimination of $\tilde{v}H(S)$ from Eqs. (3) and (4) yields

$$\left(\nabla^2 - \frac{\mathrm{D}^2}{\mathrm{D}t^2}\right)[\tilde{p}H(S)] = \nabla\cdot[\tilde{F}\delta(S)] - \frac{\mathrm{D}}{\mathrm{D}t}[\tilde{Q}\delta(S)] \tag{5}$$

a convected-wave equation for the (sound) pressure field outside $S = 0$, driven by a surface source distribution at $S = 0$. It is noted that an externally generated incident field of small amplitude does not, to leading order, interfere with the field induced by the body outside $S = 0$. However, inside $S = 0$, there will be interaction, in particular at the body surface. This interaction will be felt in the outer field through modified conditions at the interface $S = 0$.

Anticipating the existence of a Green's function $\tilde{G}$ satisfying

$$\left(\nabla^2 - \frac{\mathrm{D}^2}{\mathrm{D}t^2}\right)\tilde{G} = -\delta(\boldsymbol{x} - \boldsymbol{\xi})\,\delta(t - \tau) \tag{6}$$

we can formally solve Eq. (5) and obtain

$$\tilde{p}H(S) = \int_{\tau}\iiint_{\xi}\left[<\nabla_0\tilde{G}\cdot\tilde{F}> - \frac{\mathrm{D}\tilde{G}}{\mathrm{D}\tau}\tilde{Q}\right]\delta(S)\,\mathrm{d}\xi\,\mathrm{d}\tau \tag{7}$$

This equation is the generalization of the classical Kirchhoff-Helmholtz theorem (e.g., Ref. 6) for the acoustic pressure of a source region in a uniform mean flow. Note that Eq. (7) has been derived without the assumption of an irrotational velocity perturbation field.

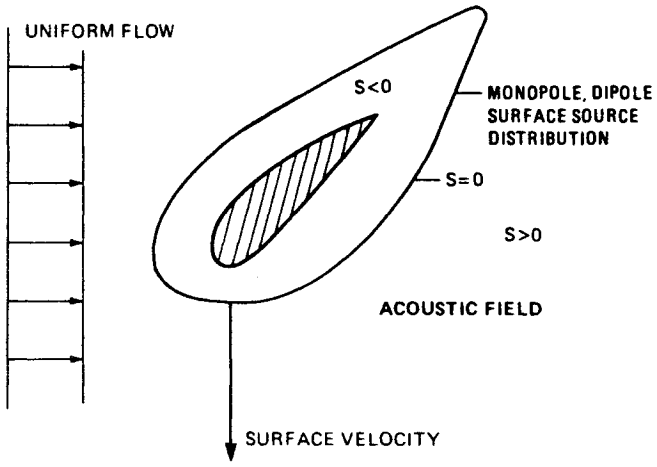


**Fig. 2 Generalized Kirchhoff-Helmholtz description of acoustic field of a body moving in uniform flow.**

There are some good reasons to make a distinction between the fields driven by the force term and the displacement term. Therefore, we define

$$\tilde{p}_F H(S) = \int_{\tau}\iiint_{\xi} <\nabla_0\tilde{G}\cdot\tilde{F}(\xi,\tau)>\,\delta(S)\,\mathrm{d}\xi\,\mathrm{d}\tau \tag{8a}$$

$$\tilde{p}_Q H(S) = -\int_{\tau}\iiint_{\xi}\frac{\mathrm{D}\tilde{G}}{\mathrm{D}\tau}\,\tilde{Q}(\xi,\tau)\,\delta(S)\,\mathrm{d}\xi\,\mathrm{d}\tau \tag{8b}$$

To compute the interaction of the sound field with another body, we need the induced velocity rather than the pressure since the boundary condition at the foreign body surface is with respect to the normal velocity. A similar elimination process as used for the pressure again leads to an inhomogeneous convected-wave equation; however, now with an additional, linear volume source term $[\nabla\times(\nabla\times\tilde{v})]\,H(S)$ next to a surface source distribution at $S = 0$. This volume source explicitly shows the effect of vorticity on the velocity field and forces us to deform the surface $S$ in order to enclose all induced vorticity. In many cases, this would imply an extension of the surface to infinity downstream that may be impractical.

Therefore, we will follow a different approach in which the effect of linear vorticity is included analytically and in which the surface $S$ can be taken the same as in the calculation of the pressure. Let us define Fourier-transformed variables

$$\begin{bmatrix}\hat{v}\\ \hat{p}\\ \hat{F}\end{bmatrix} = \int_{-\infty}^{\infty}\iint \exp\,[-i(\omega t + \alpha x)]\begin{bmatrix}\tilde{v}H(S)\\ \tilde{p}H(S)\\ \tilde{F}\,\delta(S)\end{bmatrix}\mathrm{d}x\,\mathrm{d}t$$

Now consider the momentum equation (Eq. 4) and take Fourier transforms in time and axial direction. Then, the velocity in $(\alpha, \omega)$ space is found to be

$$\hat{v}_F = \frac{1}{i(\omega + M\alpha)}\left[\hat{F} - \left(i\alpha\boldsymbol{i}_x + \boldsymbol{i}_r\frac{\partial}{\partial r} + \boldsymbol{i}_\theta\frac{\partial}{r\partial\theta}\right)\hat{p}_F\right] \tag{9a}$$

$$\hat{v}_Q = \frac{-1}{i(\omega + M\alpha)}\left(i\alpha\boldsymbol{i}_x + \boldsymbol{i}_r\frac{\partial}{\partial r} + \boldsymbol{i}_\theta\frac{\partial}{r\partial\theta}\right)\hat{p}_Q \tag{9b}$$

where $(x, r, \theta)$ is a cylindrical coordinate system (Fig. 3), which is not essential at this point but has been chosen in anticipation of the application to propellers. In Eqs. (9a) and (9b), the

velocity is exclusively in ($S = 0$) surface quantities. For $\hat{F}$, this is immediately clear through the occurrence of $\delta(S)$ in its defining integral, whereas for $\hat{p}_F$ and $\hat{p}_Q$, this becomes evident when we consider the aforementioned Eqs. (8a) and (8b). Upon evaluation of $\hat{F}$, $\hat{p}_F$, and $\hat{p}_Q$, the velocity in physical space and time is found by applying the appropriate inverse transforms. Thus,

$$\tilde{v}_F H(S) = \frac{1}{(2\pi)^2} \iint_{-\infty}^{\infty} \exp[i(\omega t + \alpha x)]\, \hat{v}_F(\alpha, r, \theta, \omega)\, d\alpha\, d\omega \tag{10a}$$

$$\tilde{v}_Q H(S) = \frac{1}{(2\pi)^2} \iint_{-\infty}^{\infty} \exp[i(\omega t + \alpha x)]\, \hat{v}_Q(\alpha, r, \theta, \omega)\, d\alpha\, d\omega \tag{10b}$$

This pair of equations can be considered as the generalized Kirchhoff-Helmholtz theorem for the velocity.

**Fundamental Solution**

The actual calculation of pressure and velocity outside the surface $S = 0$ requires a Green's function $\tilde{G}$, or fundamental solution, satisfying Eq. (6). Its classical representation is given by

$$\tilde{G} = \delta(T - R)/4\pi R \tag{11}$$

where

$$T = \beta(t - \tau) + M(x - \xi)/\beta$$

$$R = \sqrt{[(x - \xi)/\beta]^2 + r^2 + \rho^2 - 2r\rho\cos(\theta - \varphi)}$$

This representation has been used both in convective and nonconvective ($M = 0$) form by many investigators of propeller acoustics. For bodies of arbitrary shape in nonuniform motion, it is most appropriate, but for the special geometry and motion of propeller blades, an alternative representation of Green's function has certain advantages. This representation is obtained by taking (formally) the following integral transforms of Eq. (6):

$$\int_{\varphi-\pi}^{\varphi+\pi} \iint_{-\infty}^{\infty} \int_{0}^{\infty} \exp[-i(n\theta + \omega t + \alpha x)]$$

$$\times rJ_n(\gamma r)[\text{Eq. (6)}]\, dr\, dx\, dt\, d\theta$$

which yields the following expression for Green's function in wave number space ($n$, $\alpha$, $\gamma$, $\omega$):

$$\hat{\tilde{G}}_n(\alpha, \gamma, \omega | \xi, \rho, \varphi, \tau) = \frac{\exp[-i(n\varphi + \omega\tau + \alpha\xi)]\, J_n(\gamma\rho)}{\gamma^2 + \alpha^2 - (\omega + M\alpha)^2} \tag{12}$$

where $J_n$ denotes the Bessel function of the first kind and order $n$. After carrying out the inverse transforms, we obtain for Green's function in physical space

$$\tilde{G}(x, r, \theta, t | \xi, \rho, \varphi, \tau) = \frac{1}{(2\pi)^2} \sum_{n=-\infty}^{\infty} \exp[in(\theta - \varphi)]$$

$$\times \int_{-\infty}^{\infty} \exp[i\omega(t - \tau)] \int_{0}^{\infty} \gamma \frac{J_n(\gamma r)\, J_n(\gamma\rho)}{2i\kappa(\gamma, \omega)}$$

$$\times \exp\left\{\frac{i(x - \xi)}{\beta^2}[M\omega - \text{sgn}(x - \xi)\kappa(\gamma, \omega)]\right\} d\gamma\, d\omega \tag{13}$$

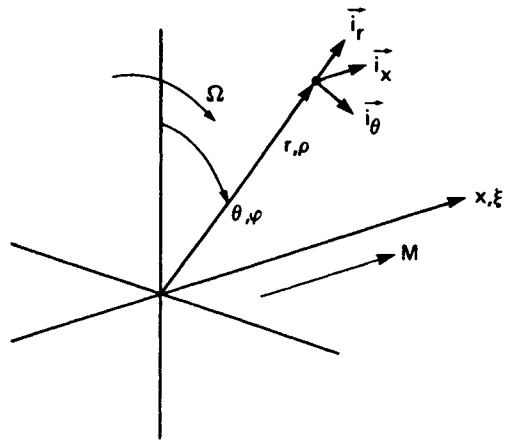


**Fig. 3 Coordinate system.**

where $\kappa(\gamma, \omega) = \sqrt{\omega - \beta\gamma}\ \sqrt{\omega + \beta\gamma}$ with the square roots defined as principal values with branch cuts such that $\text{Im}\ \kappa(\gamma, \omega) \leq 0$. It may be noted that the series in Eq. (13) does not converge normally but is to be considered a generalized function. Indeed, then the expression of Eq. (13) is equivalent to that of Eq. (11).

To obtain Eq. (13), the inverse transform $\alpha \rightarrow x$ has been performed analytically by integrating along a contour just above the real axis for $\alpha > M\omega/\beta^2$ and just below for $\alpha < M\omega/\beta^2$ in order to select the causal solution. Alternatively, the inverse transform $\gamma \rightarrow r$ can be done first analytically, leaving the transform $\alpha \rightarrow x$ for numerical integration. Then, a formulation similar to those of Goldstein,[15] Kondo,[16] and Hanson[3] is obtained.

To solve pressure and velocity from Eqs. (8) and (10), it is convenient to derive first solutions for an impulsive point force and an impulsive point displacement before integrating over the source region.

**Propeller Acoustic Field**

*Geometry*

So far, the theory is applicable to any body, moving in an arbitrary way through a flow that is uniform at infinity. From now on, we will restrict ourselves to propellers with a constant rotational speed Ω (Fig. 3). The propeller tip radius is taken as characteristic length on which the space coordinates are made dimensionless. First, the function $S_j(x, t)$ for the $j$th propeller blade is chosen as the parabola in $\theta$

$$S_j(x, r, \theta, t) = \left[\theta - \left(\Omega t + \frac{\varphi_0^\ell + \varphi_0^u}{2} + j\frac{2\pi}{B}\right)\right]^2 - \left(\frac{\varphi_0^\ell - \varphi_0^u}{2}\right)^2 \tag{14}$$

where $B$ is the number of blades and $\varphi_0^\ell(x, r)$ and $\varphi_0^u(x, r)$ are the lower and upper angular coordinates of the surface $S = 0$ (Fig. 4). Now at the surface $S = 0$,

$$\nabla S^\ell = \left(\varphi_0^\ell - \varphi_0^u\right)\left(-\frac{\partial\varphi_0^\ell}{\partial x}, -\frac{\partial\varphi_0^\ell}{\partial r}, \frac{1}{r}\right) \tag{15a}$$

$$\nabla S^u = -\left(\varphi_0^\ell - \varphi_0^u\right)\left(-\frac{\partial\varphi_0^u}{\partial x}, -\frac{\partial\varphi_0^u}{\partial r}, \frac{1}{r}\right) \tag{15b}$$

Note that in the ($x$, $r$, $\theta$) system, these vectors are independent of the angular coordinate $\theta$.

In general, we have for a point $x(t)$ on the surface $S = 0$ for all $t$ $S[x(t), t] = 0$, and so

$$\frac{d}{dt} S[x(t), t] = \left[\frac{\partial S}{\partial t} + \left\langle \frac{dx(t)}{dt} \cdot \nabla S \right\rangle\right]_{S=0} = 0$$

In the present problem, the surface velocity

$$\frac{dx(t)}{dt} = \Omega r i_\theta$$

and hence,

$$\frac{\partial S^\ell}{\partial t} = -\Omega\left(\varphi_0^\ell - \varphi_0^u\right) \tag{16a}$$

$$\frac{\partial S^u}{\partial t} = \Omega\left(\varphi_0^\ell - \varphi_0^u\right) \tag{16b}$$

Finally, from the properties of the delta function (e.g., Ref. 17), we have

$$\delta[S_j(\boldsymbol{x}, t)] = \left(\delta\left\{\theta - \left[\Omega t + \varphi_0^\ell(x, r) + j\frac{2\pi}{B}\right]\right\} + \delta\left\{\theta - \left[\Omega t + \varphi_0^u(x, t) + j\frac{2\pi}{B}\right]\right\}\right)\Big/\left[\varphi_0^\ell(x, r) - \varphi_0^u(x, r)\right] \tag{17}$$

*Discrete Tone Field*

In principle, any propeller acoustic field can be computed by means of the foregoing expressions. In practice, however, one makes a distinction between discrete tone propeller sound and broadband noise generated by turbulence in the flow along the blades. If broadband noise is significant, one is usually interested in the power spectral density of the sound rather than in its time signature. This admits some simplifications in the calculation of the broadband noise field.

In most applications, however, discrete propeller tones will dominate the generated sound. Then, circumferential periodicity permits us to write for pressure and velocity at the surface $S = 0$

$$\begin{bmatrix}\tilde{p}_j \\ \tilde{\boldsymbol{v}}_j\end{bmatrix} = \sum_\ell \exp(i\omega_\ell t)\sum_k \exp\left(ikj\frac{2\pi}{B}\right)\begin{bmatrix}p_{\ell,k,0} \\ \boldsymbol{v}_{\ell,k,0}\end{bmatrix} \tag{18}$$

where $\ell = 0$ refers to steady conditions, i.e., $\omega_0 = 0$.

If we use Eq. (18) the inverse transform to the time domain can be carried out analytically, whereas the summation over the blades is performed using the summation rule for geometric series. Then, we obtain for the discrete tone field

$$\tilde{p}_F = -\frac{B}{2\pi}\sum_\ell\sum_k \exp(i\omega_{\ell,k}t)\exp(ik\theta)\sum_{n=-\infty}^{\infty}\exp[inB(\Omega t - \theta)] \times \int_0^\infty \frac{\gamma J_m(\gamma r)}{2\kappa(\gamma, \omega_n)}\int_{r_1}^{r_2} J_m(\gamma\rho) \times \int_{x_1(\rho)}^{x_2(\rho)} \exp\left\{\frac{i(x-\xi)}{\beta^2}[M\omega_n - \operatorname{sgn}(x-\xi)\kappa(\gamma, \omega)]\right\} \times \langle \boldsymbol{b}_m^*(x-\xi, \rho, \gamma, \omega_n)\cdot\left\{\exp[-im\varphi_0^\ell(\xi, \rho)]\, f_{\ell,k}^\ell(\xi, \rho) - \exp[-im\varphi_0^u(\xi, \rho)]\, f_{\ell,k}^u(\xi, \rho)\right\}\rangle \, d\xi\, d\rho\, d\gamma \tag{19}$$

where

$$\omega_{\ell,k} = \omega_\ell - k\Omega$$

$$\omega_n = \omega_{\ell,k} + nB\Omega$$

$$m = k - nB$$

$$f_{\ell,k} = \boldsymbol{g}(\xi, \rho)p_{\ell,k,0}(\xi, \rho) - \rho\left(\Omega + M\frac{\partial\varphi_0}{\partial\varphi}\right)\boldsymbol{v}_{\ell,k,0}(\xi, \rho)$$

where the normal vector $\boldsymbol{g}(\xi, \rho) = [-\rho(\partial\varphi_0/\partial\varphi), -\rho(\partial\varphi_0/\partial\rho), 1]$ and $x_1(\rho)$ and $x_2(\rho)$ are axial coordinates of the $S = 0$ surface and $r_1$, $r_2$, its radial extremes.

Furthermore,

$$\tilde{p}_Q = -\frac{B}{2\pi}\sum_\ell\sum_k \exp(i\omega_{\ell,k}t)\exp(ik\theta)\sum_{n=-\infty}^{\infty}\exp[inB(\Omega t - \theta)] \times \int_0^\infty \frac{\gamma J_m(\gamma r)}{2\kappa(\gamma, \omega_n)}\int_{r_1}^{r_2} Jm(\gamma\rho) \times \int_{x_1(\rho)}^{x_2(\rho)} \exp\left\{\frac{i(x-\xi)}{\beta^2}[M\omega_n - \operatorname{sgn}(x-\xi)\kappa(\gamma, \omega_n)]\right\} \times \frac{\omega_n - M\operatorname{sgn}(x-\xi)\kappa(\gamma, \omega_n)}{\beta^2}\left\{\exp[-im\varphi_0^\ell(\xi, \rho)]q_{\ell,k}^\ell(\xi, \rho) - \exp[-im\varphi_0^u(\xi, \rho)]\, q_{\ell,k}^u(\xi, \rho)\right\} d\xi\, d\rho\, d\gamma \tag{20}$$

where

$$q_{\ell,k} = -\langle \boldsymbol{g}(\xi, \rho)\cdot\boldsymbol{v}_{\ell,k,0}(\xi, \rho)\rangle + \rho\left(\Omega + M\frac{\partial\varphi_0}{\partial\xi}\right)p_{\ell,k,0}(\xi, \rho)$$

In a similar way, the discrete tone velocity fields are found to be

$$\tilde{\boldsymbol{v}}_F = \frac{B}{2\pi M}\sum_\ell\sum_k \exp(i\omega_{\ell,k}t)\exp(ik\theta)\sum_{n=-\infty}^{\infty}\exp[inB(\Omega t - \theta)] \times \int_0^\infty \gamma J_m(\gamma r)\int_{r_1}^{r_2} J_m(\gamma\rho)\int_{x_1(\rho)}^{x_2(\rho)}\Big(\exp[-im\varphi_0^\ell(\xi, \rho)] \times \left\{\exp\left[-i\frac{\omega_n}{m}(x-\xi)\right]H(x-\xi) \times \left[f_{\ell,k}^\ell - \frac{\langle \boldsymbol{c}_m^*(\rho, \gamma, \omega_n)\cdot f_{\ell,k}^\ell\rangle}{(\omega_n/M)^2 + \gamma^2}\boldsymbol{c}_m(r, \gamma, \omega_n)\right] + \beta^2\frac{\exp\{i(x-\xi)[M\omega_n - \operatorname{sgn}(x-\xi)\kappa(\gamma, \omega_n)]/\beta^2\}}{2\kappa(\gamma, \omega_n)[(\omega_n/M) - \operatorname{sgn}(x-\xi)\kappa(\gamma, \omega_n)]} \times \langle \boldsymbol{b}_m^*(x-\xi, \rho, \gamma, \omega_n)\cdot f_{\ell,k}^\ell\rangle \boldsymbol{b}_m(x-\xi, r, \gamma, \omega_n)\right\} - \exp[-im\varphi_0^u(\xi, \rho)]\left\{\exp\left[-i\frac{\omega_n}{M}(x-\xi)\right]H(x-\xi) \times \left[f_{\ell,k}^u - \frac{\langle \boldsymbol{c}_m^*(\rho, \gamma, \omega_n)\cdot f_{\ell,k}^u\rangle}{(\omega_n/M)^2 + \gamma^2}\boldsymbol{c}_m(r, \gamma, \omega_n)\right] + \beta^2\frac{\exp\{i(x-\xi)[M\omega_n - \operatorname{sgn}(x-\xi)\kappa(\gamma, \omega_n)]/\beta^2\}}{2\kappa(\gamma, \omega_n)[(\omega_n/M) - \operatorname{sgn}(x-\xi)\kappa(\gamma, \omega_n)]} \times \langle \boldsymbol{b}_m^*(x-\xi, \rho, \gamma, \omega_n)\cdot f_{\ell,k}^u\rangle \boldsymbol{b}_m \times (x-\xi, r, \gamma, \omega_n)\right\}\Big) d\xi\, d\rho\, d\gamma \tag{21}$$

$$\tilde{\boldsymbol{v}}_Q = \frac{-\beta^2 B}{2\pi}\sum_\ell\sum_k \exp(i\omega_{\ell,k}t)\exp(ik\theta)\sum_{n=-\infty}^{\infty}\exp[inB(\Omega t - \theta)] \times \int_0^\infty \frac{\gamma J_m(\gamma r)}{2\kappa(\gamma, \omega_n)}\int_{r_1}^{r_2} J_m(\gamma\rho)\int_{x_1(\rho)}^{x_2(\rho)}\exp\left\{\frac{i(x-\xi)}{\beta^2} \times [M\omega_n - \operatorname{sgn}(x-\xi)\kappa(\gamma, \omega_n)]\right\} \times \boldsymbol{b}_m(x-\xi, r, \gamma, \omega_n)\left\{\exp[-im\varphi_0^\ell(\xi, \rho)]\, q_{\ell,k}^\ell - \exp[-im\varphi_0^u(\xi, \rho)]\, q_{\ell,k}^u\right\} d\xi\, d\rho\, d\gamma \tag{22}$$

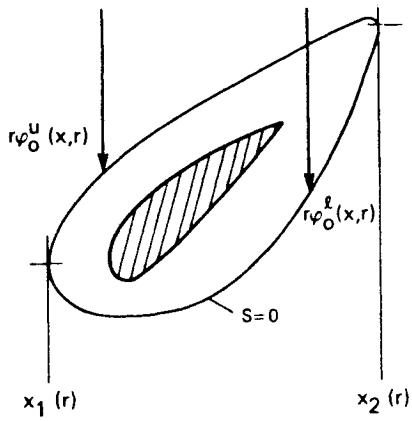


**Fig. 4 Description of $S = 0$ source surface.**

Equation (21) shows the hydrodynamic part of the velocity to depend on $x$ only through $\exp[-i(\omega_n/M)x]$, i.e., with an axial wave number $\omega_n/M$ (the hydrodynamic wave number or Strouhal number), independent of $\gamma$. Moreover, the hydrodynamic velocity extends only downstream of the point of origin. The acoustic part of the velocity has a continuous, $\gamma$-dependent spectrum and extends upstream as well as downstream. Note that the displacement velocity field, given by Eq. (22), does not have a hydrodynamic wake.

*Small Amplitude Approximation*

In the previous section, we have seen how the acoustic field of a propeller depends on the primitive flow variables at some surface $S = 0$ (moving with blades) outside of which the field behaves linearly. When the propeller blades induce relatively small perturbations in the main, uniform flow, i.e., when the propulsive efficiency is high, the surface $S = 0$ can approach the blade surfaces very closely. Then, we may take the blade surfaces themselves as the surface $S = 0$. In this approximation, the source terms can be simplified by using the boundary condition at the blade surfaces

$$<\nabla S \cdot \tilde{v}_{\text{blade}}> = <\nabla S \cdot (Mi_x + \tilde{w} + \tilde{v})> \tag{23a}$$

where $\tilde{w}$ denotes a small amplitude, incident distortion field. Rearrangement of Eq. (23a) yields

$$r\left(\Omega + M\frac{\partial \varphi_0}{\partial x}\right) = <\boldsymbol{g}(x, r)\cdot(\tilde{w} + \tilde{v})> \tag{23b}$$

Equation (23b) shows that the second terms in both $f$ and $q$ [see Eqs. (19) and (20)], are quadratically small and can be neglected with respect to the linear first terms. Further, we will use Eq. (23b) to rewrite the first term of $q$.

Let us consider a discrete tone incident velocity field

$$\tilde{w} = \sum_\ell \sum_k \boldsymbol{w}_{\ell,k} \exp(i\omega_{\ell,k}t) \exp(ik\theta) \tag{24}$$

Then, at the surface of the $j$th blade the incident velocity

$$\tilde{w}_j = \sum_\ell \sum_k \boldsymbol{w}_{\ell,k} \exp\left\{i\left[(\omega_{\ell,k} + k\Omega)t + k\varphi_0(x, r) + kj\frac{2\pi}{B}\right]\right\} \tag{25}$$

Thus for a single component $\ell$, $k$ of the incident field, the conditions at the $j$th blade surface are just the same as at the zeroth blade, apart from a phase shift $\exp[ikj(2\pi/B)]$. Since the governing equations are now linear everywhere, the surface pressure caused by this component must also be of the form

$$\tilde{p}_{\ell,k,j} = p_{\ell,k,0}(x, r) \exp\left\{i\left[(\omega_{\ell,k} + k\Omega)t + kj\frac{2\pi}{B}\right]\right\} \tag{26}$$

The source terms in the small amplitude approximation reduce to

$$f_{\ell,k} = \boldsymbol{g}(\xi, \rho)p_{\ell,k,0}(\xi, \rho) \tag{27a}$$

$$q_{\ell,k} = \exp[ik\varphi_0(\xi, \rho)] <\boldsymbol{g}(\xi, \rho)\cdot \boldsymbol{w}_{\ell,k}(\xi, \rho)> - \rho\left(\Omega + M\frac{\partial \varphi_0}{\partial \xi}\right)\delta_{0,k}\delta_{0,\ell} \tag{27b}$$

This level of approximation has been used in the numerical computations in the present paper. It is understood that the source terms given by Eqs. (27a) and (27b), when $\ell = 0$, $k = 0$, include the source strength caused by the blade geometry in the undisturbed uniform flow.

The assumption of small amplitudes in the flowfield actually implies the blade geometry to be such that induced perturbations are small. If we make the effect of the geometrical perturbation magnitude explicit, it appears that the contribution of the first term in $q_{\ell,k}$ given by Eq. (27b) is of the second order only and may be neglected in the present approximation.

## Numerical Solution

The numerical evaluation of a harmonic pressure or velocity involves a two-dimensional surface integral over one propeller blade followed by an inverse Hankel transform over the radial wave number ($\gamma$) spectrum per component ($\ell$,$k$) of the incident field. At first glance, this seems not too difficult to perform on a modern high-speed computer. However, a simple numerical approach was found most impractical, the reason being the exponential, either oscillatory or decaying, nature of the integrands. Therefore, the general strategy has been to separate the fast varying parts from the slowly varying parts and apply appropriate splining to the latter in advance of each integration.

In the chordwise ($\xi$) direction, a piecewise analytical Filon-type integration has been used where on each (straight) segment the slowly varying part was linearly approximated. In the radial ($\rho$) integration, the reduced integrand, i.e., without the Bessel function $J_m(\gamma\rho)$, is slowly varying in $\rho$ and has been accordingly splined. Due to the occurrence of the square root function $\kappa(\gamma,\omega_n)$, the behavior with respect to $\gamma$ is not smooth but has a discontinuous derivative at $\gamma = |\omega_n|/\beta$. Therefore, the reduced integrand is splined separately on two intervals: $[0, |\omega_n|/\beta]$ and $[|\omega_n|/\beta, \infty]$. Spline variables are chosen such that transformation to these variables removes the $1/\kappa$ singularity in the subsequent integration with respect to $\gamma$. Appropriate choices are $\varphi = \arcsin(\beta\gamma/|\omega_n|)$ for the first and $\tau = \sqrt{\beta^2\gamma^2 - \omega_n^2}$ for the second interval. In this last integration, the reduced integrand, i.e, without Bessel function $J_m(\gamma r)$, is already oscillatory and requires a fairly high storage density in order to evaluate the acoustic field for a series of radial coordinates ($x$ fixed). From Eqs. (19–22), it is obvious that a rotation in the $\theta$ direction is trivial.

Further economizing of the computation of the acoustic field can be obtained from the observation that for points downstream or upstream of the extreme axial boundaries of the propeller, the $x$ dependence of the field can be taken out of the (inner) surface integral

$$\int_h^1 \cdots \int_{x_1}^{x_2} \cdots \mathrm{d}\xi\, \mathrm{d}\rho$$

Then both $x$ and $r$ only appear in the integration in $\gamma$. Since the axial extent of a propeller is usually small compared to the axial interval of interest, the foregoing procedure is applicable to most points in the field to be calculated. It also forms the appropriate formulation to derive a far-field approximation.

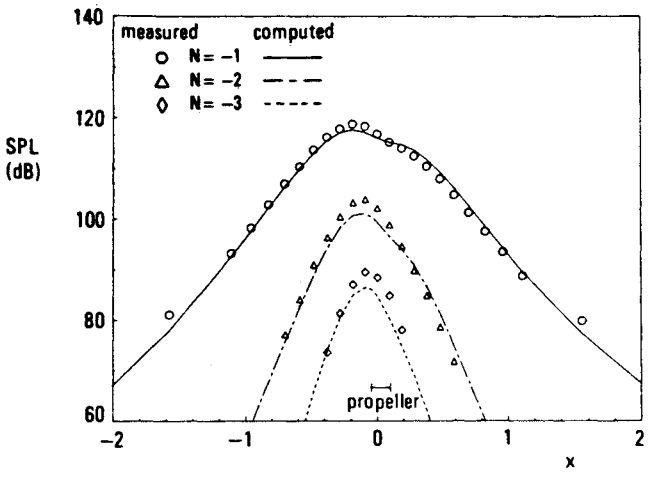


Fig. 5 Axial variation of harmonic SPL, $r = 1.323$, $M = 0.121$, $\Omega = -0.490$, $\beta_{0.7} = 28.0$ deg; moderately loaded propeller.

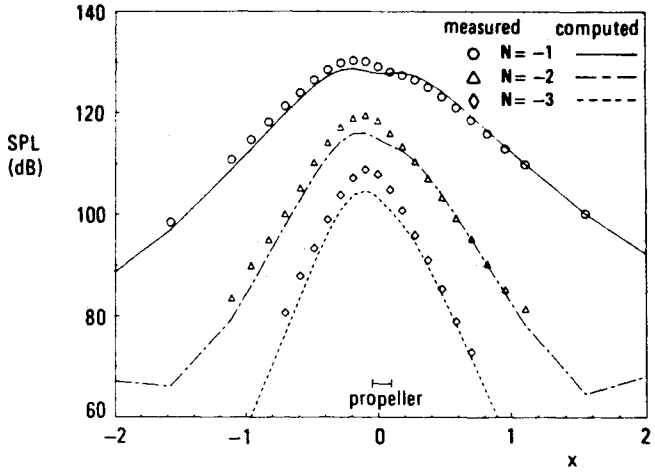


Fig. 7 Axial variation of harmonic SPL, $r = 1.323$, $M = 0.121$, $\Omega = -0.666$, $\beta_{0.7} = 28.0$ deg; heavily loaded propeller.

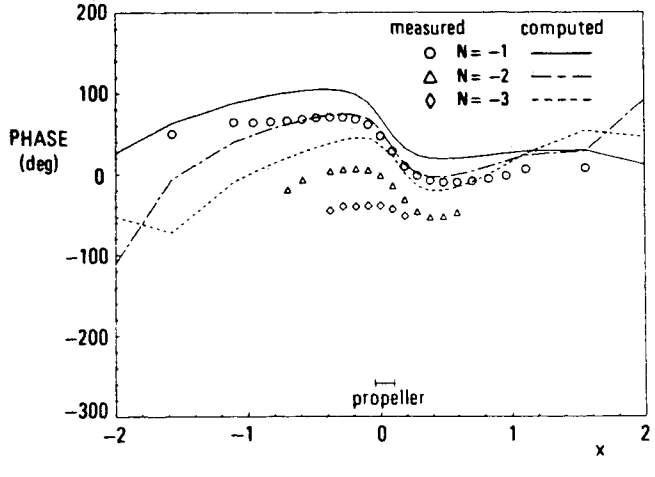


Fig. 6 Axial variation of harmonic phase, $r = 1.323$, $M = 0.121$, $\Omega = -0.490$, $\beta_{0.7} = 28.0$ deg; moderately loaded propeller.

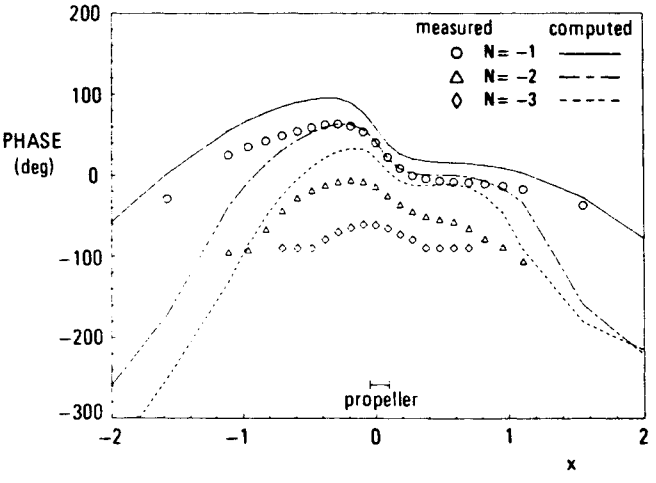


Fig. 8 Axial variation of harmonic phase, $r = 1.323$, $M = 0.121$, $\Omega = -0.666$, $\beta_{0.7} = 28.0$ deg; heavily loaded propeller.

A computer program based on the aforementioned refinements takes about 0.3 CPU s/field point to compute a harmonic pressure on a CDC 170-855 system.

## Comparison with Experiments

### Experiment

In a previous study[18] on the same problem, only a very limited comparison of the theory with experiments was included. For a real validation of the method, however, free-field experimental data over a sufficiently wide range were required. Therefore, a series of acoustic tests was carried out in the German-Dutch low-speed tunnel (DNW) in its anechoic configuration. The model was a conventional six-bladed propeller of 0.732 m diam mounted on a slender center body. Microphones installed in streamlined probes were axially traversed in the free jet at several radial distances. The aerodynamic operating conditions of the propeller also were varied over a considerable range. Since the propeller rotates in the negative direction (Fig. 3), the propeller circumferential Mach number $\Omega$ is negative. Hence, negative harmonic indices are to be taken for positive frequencies.

To obtain the blade surface pressure distribution, required as input to the acoustic calculations, a two-dimensional method[13] for the local blade section aerodynamics coupled with blade element momentum theory,[14] including the Prandtl tip relief model, was applied. For the conventional, unswept propeller used in the experiment, this procedure is expected to yield a reasonable approximation of the global aerodynamics.

### Very Near Field

Figure 5 gives the computed sound pressure level (SPL, reference pressure $2 \times 10^{-5}$ Pa) and the data measured along an axial trajectory at a radial distance $r = 1.323$ (tip radius = 1) for a moderately (blade lift coefficient 0.9 at $r = 0.7$) loaded condition of the propeller. Good agreement is observed along the major part of the interval. The small deviations close to the propeller tip are not unexpected since the approximations made in the aerodynamic modeling fall short in the tip region. The seemingly larger discrepancies for the higher harmonics are, in fact, still small if we consider the 15 dB decrease in peak level per harmonic.

The phase variation along the same axial line is plotted in Fig. 6. The computed first harmonic has a phase lead of 24 deg in the propeller plane ($x = 0$). This corresponds to 4 deg in the circumferential blade position, which is just within the measuring accuracy of the experiment. Phase shifts of the higher harmonics are roughly proportional to the harmonic number and so within the measuring accuracy too. However,

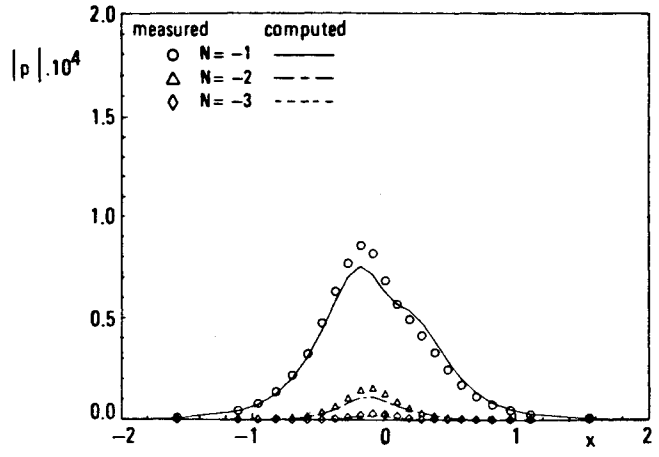


Fig. 9 Axial variation of harmonic pressure magnitude, $r = 1.323$, $M = 0.121$, $\Omega = -0.490$, $\beta_{0.7} = 28.0$ deg; moderately loaded propeller.

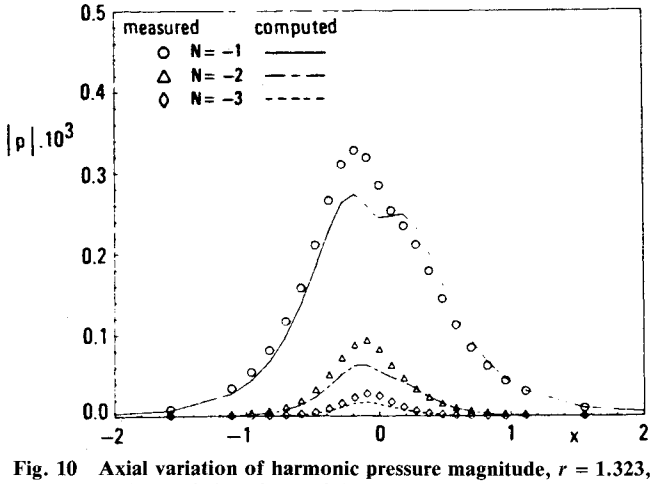


Fig. 10 Axial variation of harmonic pressure magnitude, $r = 1.323$, $M = 0.121$, $\Omega = -0.666$, $\beta_{0.7} = 28.0$ deg; heavily loaded propeller.

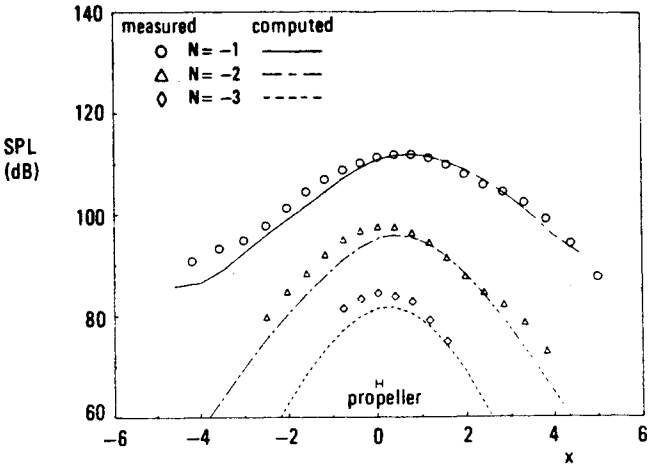


Fig. 11 Axial variation of harmonic SPL, $r = 3.890$, $M = 0.121$, $\Omega = -0.666$, $\beta_{0.7} = 28.0$ deg; heavily loaded propeller.

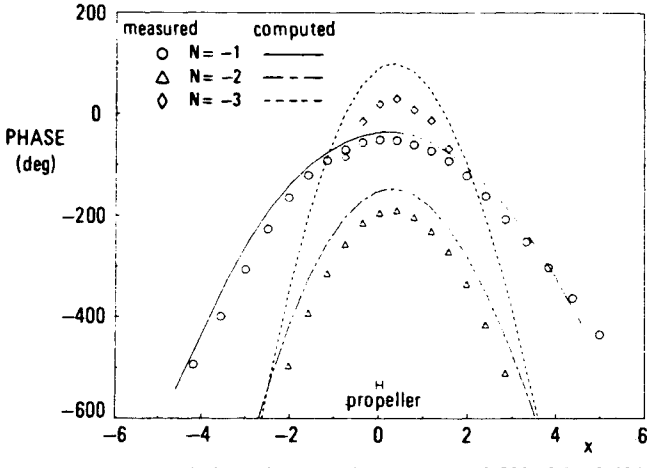


Fig. 12 Axial variation of harmonic phase, $r = 3.890$, $M = 0.121$, $\Omega = -0.666$, $\beta_{0.7} = 28.0$ deg; heavily loaded propeller.

away from the propeller plane, the phase discrepancies become significant. At the peak level position, the phase shift of the first harmonic has increased to about 33 deg. Since the distance to the propeller is very small, this phase shift can hardly be attributed to nonuniform acoustic propagation. Most probably, this shift is a result of the incomplete aerodynamic modeling of the propeller.

Figure 7 gives the SPL of a heavily loaded (blade lift coefficient 1.2 at $r = 0.7$) condition. Compared to the previous case, the peak level of the fundamental tone is about 12 dB higher. Here also, the agreement of computed and measured data is satisfactory with the theory somewhat underpredicting the measured peak level. Apart from the shift just mentioned, the phase agreement shown in Fig. 8 is as good as that in the moderately loaded case.

Because of the characteristics of the human ear, sound pressures are usually presented on a logarithmic scale. However, if the sound field drives another physical process, e.g., the vibration of an aircraft fuselage structure, a linear scale is more relevant.

Therefore, Figs. 9 and 10 present the absolute values of the acoustic pressure on a linear scale. Compared to the logarithmic dB scales, things look less favorable now. For the moderately loaded condition, there is a 14% discrepancy of the first and a 30% of the second harmonic in the neighborhood of the propeller tip. For the heavy loading, the corresponding figures are 21 and 43%. Also, the peculiar double-peak shape of the computed pressure amplitudes is not observed in the experiment.

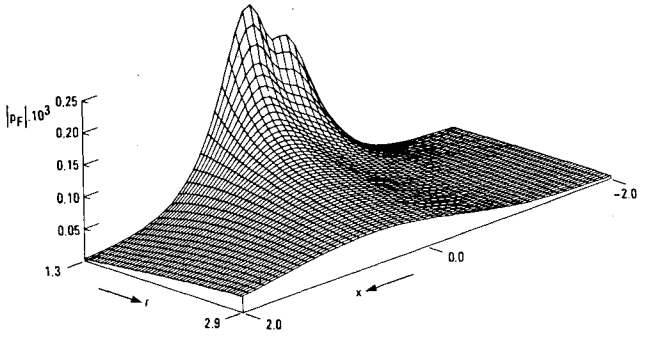


Fig. 13 First harmonic loading noise magnitude, $M = 0.121$, $\Omega = -0.666$, $\beta_{0.7} = 28.0$ deg; heavily loaded propeller.

### Near Field

Figures 11 and 12 present SPL and phase for the heavily loaded condition, but now at the larger distance $r = 3.89$. Here, the computed and measured peak levels of the dominating first harmonic agree perfectly. This supports our earlier conjecture that the discrepancies found close to the propeller tip are local, but still significant, and vanish at a larger distance. The phase correspondence is also better than in the very near field. The higher measured levels upstream of the propeller have been found to be due to spurious reflections on the microphone support.

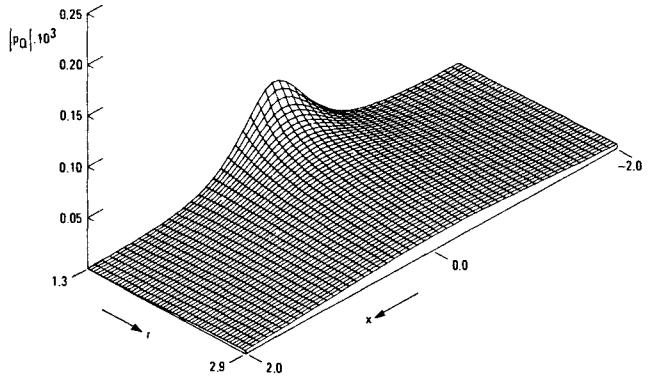


**Fig. 14 First harmonic displacement noise magnitude, $M = 0.121$, $\Omega = -0.666$, $\beta_{0.7} = 28.0$ deg; heavily loaded propeller.**

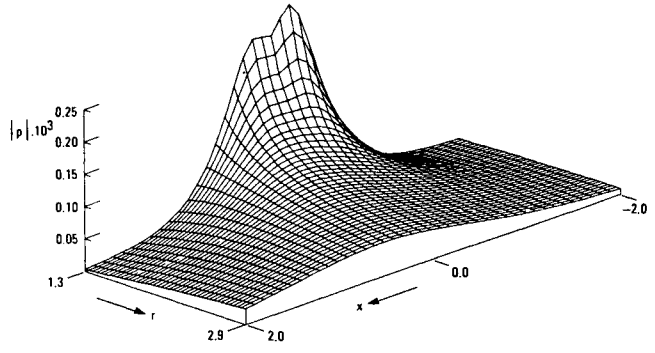


**Fig. 15 First harmonic total noise magnitude, $M = 0.121$, $\Omega = -0.666$, $\beta_{0.7} = 28.0$ deg; heavily loaded propeller.**

To give some impression of the possibilities for inspection offered by the method, Figs. 13–15 are presented. It would be very costly to obtain a similar field survey by measurement. Figure 13 shows a double peak in $|p_F|$ close to the propeller tip, whereas Fig. 14 shows a single peak in $|p_Q|$. Summation of loading noise ($p_F$) and thickness noise ($p_Q$) also yields a double peak in the pressure amplitude (Fig. 15) but by interference now with the highest peak upstream. It is noted that in this case the thickness noise is much weaker than the loading noise. The double peak is only observed close to the tip and vanishes rapidly at a larger distance.

## Concluding Remarks

In the present paper, we have analytically derived expressions for the acoustic field of a propeller in a uniform, subsonic main flow that may be perturbed by an incident unsteady, nonaxisymmetric field. The acoustic field is, in principle, described in terms of flow conditions on a surface surrounding the propeller. This surface is to be chosen such that outside of it, the perturbations on the main uniform flow are small. This generalized Kirchhoff-Helmholtz approach not only yields an acoustic pressure and velocity field but also a hydrodynamic wake, i.e., a convective velocity field with Strouhal periodicity. The present theory avoids the laborious calculation of the three-dimensional quadrupole source distribution in the more usual acoustic analogy concept.

By using a Green's function representation in separated, cylindrical coordinates, a spectral formulation resembling the modal solution for cylindrical ducts is obtained. Then, the acoustic field is conveniently expressed as a series of harmonic amplitudes. Surface integration has to be performed for one blade only since the interference effects from other blades are analytically included. Consequently, a large number of field points can be computed economically, which makes the method appropriate to generate the incident acoustic field in the problem of sound diffraction by a fuselage.

A comparison of the method with experimental data obtained from an isolated propeller in an anechoic wind tunnel shows good overall agreement both in amplitude and phase. Only close to the propeller tip do some discrepancies appear. Most probably, these are due to approximations in the aerodynamic modeling. Indeed, since the aeroacoustic modeling can be done exactly, improvement of acoustic field calculations almost entirely depends on the availability of more accurate aerodynamic input data.

## Acknowledgments

The present investigation was sponsored by the Netherlands Agency for Aerospace Programs (NIVR). The computer programming was carried out by C. H. Hofstra. Aerodynamic data were computed by H. A. Sytsma, while the experimental work in the wind tunnel was done under the supervision of T. Zandbergen.

## References

[1]Metzger, F. B. and Rohrbach, C., "Benefits of Blade Sweep for Advanced Turboprops," *Journal of Propulsion and Power,* Vol. 2, Nov.-Dec. 1986, pp. 534–540.

[2]Farassat, F., "Prediction of Advanced Propeller Noise in the Time Domain," *AIAA Journal,* Vol. 24, April 1986, pp. 578–584.

[3]Hanson, D. B., "Near-Field Frequency-Domain Theory for Propeller Noise," *AIAA Journal,* Vol. 23, April 1985, pp. 499–504.

[4]Ffowcs-Williams, J. E. and Hawkings, D. L., "Sound Generation by Turbulence and Surfaces in Arbitrary Motion," *Philosophical Transactions of the Royal Society of London,* Series A, Vol. 264, 1969, pp. 321–342.

[5]Lighthill, M. J., "On Sound Generated Aerodynamically. I. General Theory," *Proceedings of the Royal Society of London,* Series A, Vol. 221, 1952, pp. 564–587.

[6]Pierce, A. D., *Acoustics. An Introduction to Its Physical Principles and Applications,* Series in Mechanical Engineering, McGraw-Hill, New York, 1981.

[7]Lyrintzis, A. S. and George, A. R., "Calculation of Far-Field Noise Using the Kirchhoff Method," AIAA Paper 87-2673, Oct. 1987.

[8]Isom, M., Purcell, T. W., and Strawn, R. C., "Geometrical Acoustics and Transonic Helicopter Sound," AIAA Paper 87-2748, Oct. 1987.

[9]Farassat, F., "Quadrupole Source in Prediction of the Noise of Rotating Blades—A New Source Description," AIAA Paper 87-2675, Oct. 1987.

[10]Gutin, L., "On the Sound Field of a Rotating Propeller," NACA TM 1195, 1948 (from *Phys. Zeitschrift der Sowjetunion,* Bd. 9, Heft 1, 1936, pp. 57–71).

[11]Tanna, H. K., Burrin, R. H., and Plumblee, H. E., "Installation Effects on Propeller Noise," AIAA Paper 80-0993, June 1980.

[12]Durbin, P. A. and Groeneweg, J. F., "Rough Analysis of Installation Effects on Turboprop Noise," NASA TM 82924, Nov. 1982.

[13]Collyer, M. R. and Lock, R. C., "Improvements to the Viscous Garabedian and Korn (VGK) Method for Calculating Transonic Flow Past an Aerofoil," Royal Aircraft Establishment, Farnborough, England, RAE TR 78039, 1978.

[14]Labrujère, Th. E. and Kassies, A., " 'SIMPROP,' A System for Simple Aerodynamic Analysis of Propellers in Axial Flow. Description of Method and Users' Guide," National Aerospace Lab., Amsterdam, the Netherlands, NLR TR 84128 U, Dec. 1984.

[15]Goldstein, S., "On the Vortex Theory of Screw Propellers," *Proceedings of the Royal Society of London,* Series A, Vol. 123, 1929, pp. 440–465.

[16]Kondo, K., "On the Potential-Theoretical Fundamentals of the Aerodynamics of Screw Propellers at High Speed," *Journal of the Faculty of Engineering, University of Tokyo,* Vol. XXV, No. 1, 1957, pp. 1–39.

[17]Kanwal, R. P., *Generalized Functions: Theory and Technique,* Academic Press, New York, 1983.

[18]Schulten, J. B. H. M., "Aeroacoustics of Wide-Chord Propellers in Non-Axisymmetric Flow," AIAA Paper 84-2304, Oct. 1984.